

Hub effect in propeller design and analysis

S. Brizzolara¹, S. Gaggero², D. Grassi³

¹ Visiting Associate Professor, Department of Mechanical Engineering, MIT, Cambridge, USA

² Department of Naval Architecture (DITEN), Università di Genova, Genova, Italy

³ ZF Marine, Arco di Trento, Italy

ABSTRACT

The importance of considering hub effects in the design, optimization and verification of marine propellers is discussed in the paper. Different design variants of optimum moderately loaded modern propellers are obtained by means of fully numerical lifting line/surface vortex lattice methods, with and without hub effect. Anti-symmetric vortex images are used to implement the effects of the hub by the vortex lattice codes. Classical parametric lifting surface corrections are also used to correct pitch and camber. Global as well as local (pressure distribution) hydrodynamic properties of the propellers are compared as obtained from a fully numerical lifting surface method, a boundary element method and a finite volume RANS solver, referred to as the closest model of the real flow. The comparison permits to highlight the undesired consequences which a designer should expect if an inadequate or inconsistent hub modeling is used in some part of the propeller design process. Indeed, the best propeller design, in terms of efficiency, thrust matching and shock-free condition on its inner section is found when the hub effect is considered by all the numerical methods used for design.

Keywords

Marine Propeller Design, Hub Effect, Lifting Line Vortex Lattice, Lifting Surface, Panel Method, RANSE.

1 INTRODUCTION

Modern marine propeller design still relies on the lifting line theory, at least in the first design stage when the optimum circulation distribution needs to be selected. Actually the majority of the contemporary design codes are still based on the classical of Eckhardt and Morgan (1955) propeller design method that proposes a good engineering solution to the original problem definition valid for lightly or moderately loaded propellers developed by Lerbs (1952), who completely ignored the presence of the hub.

McCormick (1955) first proved that the effect of finite hub radius in the range of 0.2-0.4 times the propeller radius effectively has a non-negligible influence on the optimum circulation distribution, found according to the Betz optimum condition. In his analysis McCormick

modeled the effect of an infinitely long cylindrical hub by imposing a zero radial velocity at its radial position, thus permitting to find a non-null circulation that, summing up at the end of the hub cap forms the hub vortex in the propeller wake. This boundary condition at the blade root (hub surface) seems closer to reality than the zero-circulation condition imposed by Tachmindji (1956) and Tachmindji and Milam (1957), considering the evidence from the experiments on model propellers: in fact the hub at least partially does have a wall effect and maintains a finite circulation at the hub, which according to McCormick changes with the number of blades, propeller load and advance ratio. Finite circulation at the hub means that each blade releases a trailing vortex at the root section. These trailing vortices are summing up at the hub trailing edge into a single, stronger hub vortex. This is the physical evidence well highlighted for example by Kerwin (2007). The hub vortex is characterized by a viscous core that prevents the ideal pressure recovery on the stern closure of the hub cap, inducing an additional drag force (effective thrust deduction). Lifting line methods with hub effects must correctly consider this additional drag when optimizing the circulation for optimum propeller efficiency, as first pointed out by Wang (1985), who proposes a simplified method for calculating this added drag. Kerwin and Leopold (1964) were the first to adopt a 2D image vortex method to represent the symmetric flow condition imposed by the cylindrical surface of the hub at the blade position, effectively imposing the same boundary condition of infinitely long cylinder used by McCormick in his analytical method. Sanchez-Caja (1988) presented a higher fidelity lifting line model of a propeller, where hub effects are represented by means of quadrilateral panels distributed on the (cylindrical) hub surface, demonstrating the almost perfect correspondence with the less computationally expensive vortex image method proposed by Kerwin and Leopold (1964). Coney (1989) discusses in a certain detail all these different approximated models, in the end selecting the one proposed by Kerwin and Leopold (1964) for the development of his fully numerical lifting line design code. Also Kimball and Epps (2010) in OpenProp, a

design, optimization and analysis code, based on the minimization algorithm of Coney (1989) again use the image vortex analogy by Kerwin and Leopold for the inclusion of the hub influence.

In spite of the apparently well proven image method for lifting line design methods, what about later propeller design phases, namely lifting surface corrections and what about the real correlation of the theoretical propeller design with higher fidelity methods, used in the final design stage for optimization?

This paper aims to bring some light also on these aspects, as important as the early design codes for obtaining a consistent blade design at the hub. In fact, few validation or verification studies have been published about the consequences of the hub proximity corrections on the final design and hydrodynamic global/local performance of the propeller. It is fundamental other than theoretically correct that consistent tools are used all along the different stages of the propeller design and optimization. Unfortunately, routine design procedures do not always reflect this consistency, for instance, still widely using parametric lifting surface corrections, taken from the systematic calculation of Morgan et al. (1968), in which hub effects are simply neglected. Another more practical technique is to set hub radius to zero in lifting line codes (Lerb's method) and then empirically correcting the optimum circulation at the blade inner radii to prevent the locally negative angles of attack there.

Additionally, parametric lifting surface corrections does not allow for modern skew distributions which can be properly considered in fully numerical methods. Knowing the level of approximation of the various idealized models, where do they stand with respect to reality? What is the difference in terms of final propeller geometry and hydrodynamic performance? Which model is able to get closer to the "real" best propeller?

It is clear that the answer to these practical questions can only come from a systematic study in which the various models are applied and verified on the performance of the designed propellers: this is the main scope of this work. In this paper, in fact, we present a systematic investigation of the effect of the hub proximity at all levels of the propeller numerical design and verification procedures from the initial design to the final verification with higher fidelity CFD codes.

We present also the theoretical aspects of a complete suite of design and analysis codes in which a consistent theoretical model of the hub effect has been implemented. The numerical methods used in this study range from lifting line methods (Gaggero et al., 2011) used for definition of the optimum circulation of single or multi-stage propellers, to exact lifting surface methods (Tincani et al. 2008) with and without hub modeling used for camber and pitch corrections, to vortex lattice methods (Grassi and Brizzolara, 2007) or 3D panel methods used in the latest design stage for verification (Gaggero and Brizzolara, 2009) or for final optimization (Brizzolara et al., 2009, Bertetta et al. 2012).

Through a real design example, we will show the consequences of the neglected hub effects in an element of the propeller lifting line / lifting surface design method, such as for instance in using a zero hub radius lifting line theory (original Lerbs' method) or using a correct lifting line design method with hub effect and a non-consistent lifting surface theory for correcting pitch and camber distribution at the hub. Main conclusions gathered from the systematic application of the various design methods are drawn on the resulting propeller geometry and will be finally validated through the analysis of the propeller designed variants obtained with the different methods.

2 THEORETICAL BACKGROUND

The hub proximity effect has been systematically investigated following the whole propeller numerical design and analysis process, applying a wide range of hydrodynamic models from lifting line to RANS solvers. The optimal circulation distribution has been computed using a fully numerical lifting line code (Coney, 1989, Gaggero et al. 2011) which includes the influence of the hub wall. First tentative geometries have been corrected for lifting surface effects, using both the parametric formulae of Morgan et al. (1968) and a specifically developed numerical lifting surface approach (Tincani et al., 2008). Corrected geometries have been analyzed by a lifting surface and a panel methods developed by authors, while RANS computations are finally used for the verification of the numerical design, as a surrogate of experimental tests, the accuracy of the solver being demonstrated in different occasions (e.g. Brizzolara et al., 2008).

2.1 Design by Numerical Lifting Line Code

The well-established design approach based on the Betz criterion (Lerbs, 1952) of minimum energy loss of the flow downstream the propeller has been extensively applied for the design of lightly and moderately loaded propellers operating in uniform and non-uniform inflow: the optimal, continuous, load distribution over the blade radius is represented by a sine series, whose coefficients are the unknown of the problem. When, instead, a fully numerical lifting line design approach as, for instance, that proposed by Coney (1989) is adopted, the bounded circulation is replaced by a set of superimposed helical horseshoe vortices of constant intensity, whose strength has to be determined as the solution of a constrained minimization problem. In this model the addition of the hub effect is straightforward. If trailing helical vortices of sufficiently high pitch are considered, the zero radial velocity condition on the hub radius can be satisfied adopting anti-symmetric vortex images (in the cylindrical reference systems) to those representing the blade (Kerwin and Leopold, 1964), having a radius r_i equal to:

$$r_i = \frac{r_h^2}{r} \quad (1)$$

in which r_h is the hub radius and r the radius of the corresponding blade or wake vortex. This system of discrete vortex segments, bound to the lifting lines and trailed in the wake, induces axial, tangential and radial velocity components on each control points of the lifting

line where boundary conditions are enforced. These self-induced velocities are computed applying the Biot-Savart law as the contribution, on each i control point, of all the m horseshoe vortexes modeling each blade (M) and the relative image (M_h) arrangement, with the usual notation for the axial, tangential and radial influence coefficients A_{im} , T_{im} and R_{im} :

$$\begin{aligned} u_a(r_i) = u_{ai} &= \sum_{m=1}^{M+M_h} A_{im} \Gamma_m \\ u_t(r_i) = u_{ti} &= \sum_{m=1}^{M+M_h} T_{im} \Gamma_m \\ u_{tr}(r_i) = u_{ri} &= \sum_{m=1}^{M+M_h} R_{im} \Gamma_m \end{aligned} \quad (2)$$

With this discrete model, the hydrodynamic thrust and torque characteristics of the propeller operating in a spatial axial, radial and tangential non uniform inflow ($V_a; V_r; V_t$) can be computed by adding the contribution of each discrete vortex on the lifting line. Assuming (Anderson, 1997) that the bound vortexes lie on the “skewed” and “raked” mid-chord line (skew and rake distributions are a given input to the design procedure), described by the curvilinear coordinate s along the tangent vector ($\partial x/\partial s; \partial r/\partial s; r\partial\theta/\partial s$) represented in figure 1, the ideal delivered thrust and torque can be computed using the expressions of equation 3:

$$\begin{aligned} T &= \rho Z \int_{s_h}^s \Gamma(s) \left[\frac{\partial r}{\partial s} (\omega r(s) - u_t(s)) \right. \\ &\quad \left. - r \frac{\partial \theta}{\partial s} (V_r(s) + u_r(s)) \right] ds \\ Q &= \rho Z \int_{s_h}^s \Gamma(s) \cdot r(s) \left[\frac{\partial r}{\partial s} (V_a(s) + u_a(s)) \right. \\ &\quad \left. - \frac{\partial x}{\partial s} (V_r + u_r) \right] ds \end{aligned} \quad (3)$$

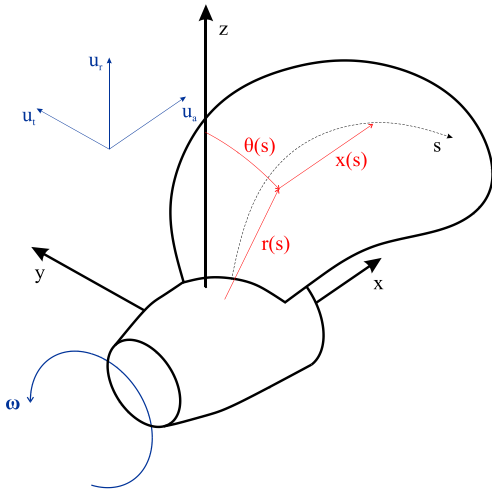


Figure 1: Propeller reference systems.

The same expression (3), written in discrete form, yields to:

$$\begin{aligned} T &= \rho Z \sum_{m=1}^M \Gamma_m \left[\frac{\partial r_m}{\partial s} (\omega r_m - u_{tm}) \right. \\ &\quad \left. - r_m \frac{\partial \theta_m}{\partial s} (V_{rm} + u_{rm}) \right] \Delta s_m \\ Q &= \rho Z \sum_{m=1}^M r_m \Gamma_m \left[\frac{\partial r_m}{\partial s} (V_{am} + u_{am}) \right. \\ &\quad \left. - r_m \frac{\partial x_m}{\partial s} (V_{rm} + u_{rm}) \right] \Delta s_m \end{aligned} \quad (4)$$

in which self-induced velocities are computed according equation 2. A variational approach provides a general procedure to identify the set of discrete circulation values Γ_m such that the propeller torque (as computed in equation 4) is minimized, being the value T_R of the requested propeller thrust a constraint. Introducing the additional unknown represented by the Lagrange multiplier λ , the problem can be solved in terms of an auxiliary function $H = Q - \lambda \cdot (T - T_R)$ requiring that its partial derivatives are equal to zero:

$$\begin{aligned} \frac{\partial H}{\partial \Gamma_m} &= 0 \quad \text{for } m = 1..M \\ \frac{\partial H}{\partial \lambda} &= 0 \end{aligned} \quad (5)$$

Carrying out partial derivatives, equation 5 leads to a nonlinear system of equations for the vortex strengths and for the Lagrange multiplier, because self-induced velocities depend, in turn, by the unknown strengths of the bound vortexes. The iterative solution of the nonlinear system is iteratively solved in order to find the optimal circulation distribution able to minimize torque satisfying the prescribed thrust. This formulation can be further improved to design highly loaded propellers and to include viscous effects. The initial horseshoe vortexes that represent the wake, frozen during the solution of equation 5 can be aligned with the velocities induced by the actual distribution of circulation and the solution iterated until convergence of the wake shape (or of the induced velocities themselves). A viscous thrust reduction, as a force acting on the direction parallel to the total velocity and thus as a function of the self-induced velocities themselves, can be furthermore added to the auxiliary function H and a further iterative procedure, each time the chord distribution of the propeller has been determined, can be also implemented. In our case, for the presented propeller designs, the devised procedure works with:

- An inner iterative approach for the determination of the optimal circulation distribution by the solution of the linearized version of equation 5,
- A second-level iterative approach to include the viscous drag on the optimal circulation distribution, by adding viscous contribution to the auxiliary function H ,
- A third-level iterative approach to include the wake alignment and improve the accuracy of induction factors.

Once the optimum circulation distribution is known the chord length at each radial position is found using the semi-empirical method described by Brizzolara et al. (2012) in case of contra rotating propeller design.

2.2 Lifting Surface Corrections

Lifting surface corrections have been applied following, first in parametric form, the well-known theory by Morgan et al. (1968) by using the polynomial representation proposed by Van Oossanen (1968), where hub effects are not present. Alternatively, the fully numerical treatment of lifting surface corrections is based on the original framework of Greeley and Kerwin (1982) and on the more general formulation of Grassi and Brizzolara (2007). This last method has been recently improved to account for the influence of the hub through the same image approach already described for the lifting line design code (1).

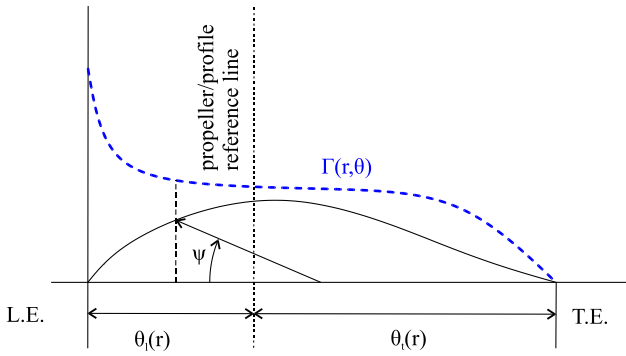


Figure 2: Local profile reference system.

A structured lattice of chordwise and spanwise discrete vortex elements and spanwise source elements is distributed over the mean blade surface. A horseshoe vortex lattice represents the propeller wake, being able to contract and align with the local flow. Once a Cartesian coordinate system fixed on the propeller and a local coordinate system on the profile (figure 2) have been defined, it is possible to derive the bound circulation distribution $\Gamma(r)$ over the radius, obtained from the lifting line design code, as the contribution of the chordwise distribution of circulation $\Gamma_r(r, \vartheta)$ on the blade mean surface in the form of a sine series for the angular coordinate Ψ (Grassi and Brizzolara, 2007, Brizzolara et al., 2012) :

$$\Gamma(r) = \int_{\vartheta_t}^{\vartheta_l} \Gamma_r(r, \vartheta) d\vartheta \quad (6)$$

Following the same convention, it is possible to derive a relation between the constant strength of the free trailing vortices ($\Gamma_f(r) = -\partial\Gamma(r)/\partial r \cdot dr$) and of the chordwise vortices with the spanwise bound circulation:

$$\Gamma_f(r) = - \int_{\vartheta_t(r)}^{\vartheta_l(r)} \frac{\partial\Gamma_r(r, \vartheta)}{\partial r} d\vartheta dr - \Gamma_r(r, \vartheta_l) \times \frac{d\vartheta_l}{dr} dr + \Gamma_r(r, \vartheta_t) \frac{d\vartheta_t}{dr} dr \quad (7)$$

$$\Gamma_f(r, \theta) = -\Gamma_r(r, \vartheta_l) \frac{d\vartheta_l}{dr} dr - \int_{\vartheta}^{\vartheta_l(r)} \frac{\partial\Gamma_r(r, \vartheta_0)}{\partial r} d\vartheta_0 dr$$

The induced velocity, for each control points on the mean blade surface, can be simply computed by the application of the Biot-Savart law to the lattice of vortex rings on the blades and in the wake (having their intensities calculated with equations 7). The influence of the blade thickness on the induced velocity field can be included by a lattice of sources, whose intensity is linearly proportional to the variation of the profile thickness along the chord. On the blade mean surface a zero normal speed condition is imposed, from which it is possible to derive a relation between the local angle of attack $\alpha(r)$, the local camber $f(r, x)$, the resultant inflow velocity $V_r(r)$, the resulting induced velocity from the lifting line $U(r)$ and the total induced velocity (vortexes and sources) normal to the blade nose-tail line $(V_{induced}(r, x))_n$:

$$\alpha(r) + \frac{\partial f(r, x)}{\partial x} = \frac{(V_{induced}(r, x))_n}{V_r(r)} - \frac{U(r)}{V_r(r)} \quad (8)$$

The iterative solution of equation (8) includes the alignment of the discrete lattice of singularities with the resulting flow in the wake and the scaling of the circulation distribution to match the prescribed thrust in order to increase the accuracy of the lifting surface (induced velocity calculation). A good correction of the camber and pitch distributions is usually obtained from this solution of (8) for single and contra-rotating propellers (Brizzolara et al., 2012) with moderate skew distributions.

2.3 Analysis Tools – Potential Flow solvers

In the framework of potential theories, a lifting surface code (Grassi & Brizzolara, 2007) and a panel method (Gaggero and Brizzolara, 2009) have been used to analyze the hydrodynamic performance of the designed propellers. A lattice of discrete vortex rings and straight line source elements (same discrete model used for lifting surface corrections) replace the continuous distribution of vorticity and sources on the mean blade surface. A set of horseshoe vortexes represents, instead, the wake. The presence of the hub, as for the lifting line design and the lifting surface corrections, is addressed as described in Kerwin and Leopold (1964): each vortex line is duplicated with an image element (equation 1) of equal and opposite strength, while image sources are included with the same sign of those distributed on the blade surface.

Our panel method uses distributions of sources and dipoles on the effective blades and hub surfaces, numerically discretized through hyperboloidal panels (Morino and Kuo, 1974), plus a distribution of dipoles in the trailing wake, equivalent, in the steady case, to the horseshoe vortexes arrangement of the lifting surface.

Boundary conditions (kinematic on the solid boundaries, Kutta at the blade trailing edge and force free condition on the trailing wake) apply for both the solvers leading to linear systems of equations for the unknowns of the potential problems (vortex rings strength on the mean lifting surfaces, dipoles strength on the blades and hub surfaces). Pressure forces are obtained from the total velocity field on the blades, while the effect of viscosity is addressed through friction corrections.

2.4 Analysis Tools – RANS

The accuracy and the efficiency of RANS solvers has increased significantly in the last years, making RANS solutions, in many engineering cases, a reliable alternative to the experimental measurements and an excellent tool to understand and visualize complex flow phenomena. In addition to lifting surface and panel methods, hence, also a commercial finite volume RANS solver (CD-Adapco, 2012) has been adopted to simulate the viscous flow around the propellers and, thereby, to have a set of reference results to validate the design methodology and to be compared with the potential results. For non-cavitating simulations, continuity and momentum equations of an incompressible fluid are satisfied:

$$\begin{cases} \nabla \cdot \mathbf{V} = 0 \\ \rho \mathbf{V} = -\nabla p + \mu \nabla^2 \mathbf{V} + \nabla \cdot \mathbf{T}_{Re} + \mathbf{S}_M \end{cases} \quad (9)$$

in which \mathbf{V} is the averaged velocity vector, p is the averaged pressure field, μ is the dynamic viscosity, is the momentum sources vector and \mathbf{T}_{Re} is the tensor of Reynolds stresses, computed in agreement with the two layers Realizable $k - \varepsilon$ turbulence model. Better description of numerical model used and validation in case of different propellers are given for instance in Brizzolara et al. (2008).

3 DESIGN ACTIVITY

3.1 Validation with Lerbs Propeller

The fully numerical lifting line design method has been validated in the case of a hubless propeller, for which a classical solution on the basis of Goldstein's induction factors is given by Lerbs (1952). Circulation distribution over the radius and self-induced axial and tangential velocity distributions are compared with the original Lerbs computations and with the results from a classical design approach based on Lerbs theory (Tincani et al. 2008) in figures 3 and 4 respectively.

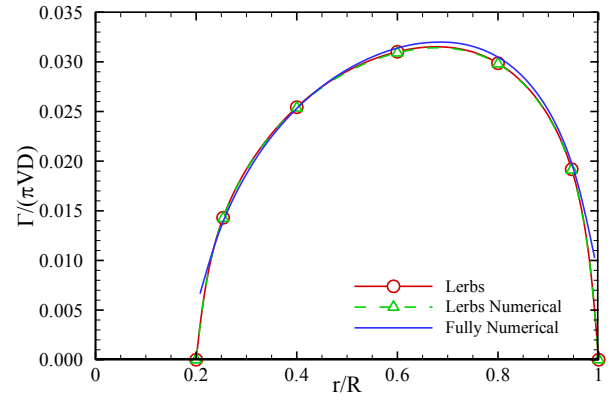


Figure 3: Computed circulation distributions for the Lerbs propeller.

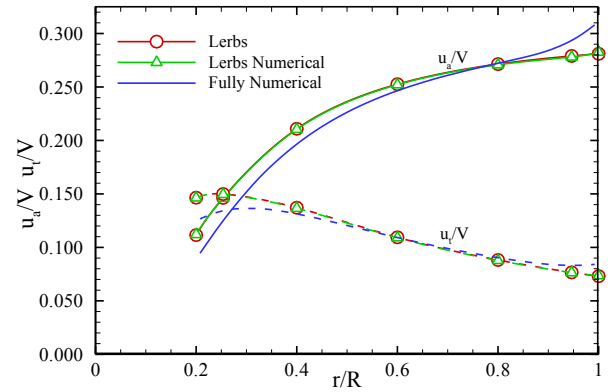


Figure 4: Computed self-induced velocity distributions for the Lerbs propeller.

Correlations are in general satisfactory. The load distribution found with the fully numerical design method significantly differs with the semi-analytical method of Lerbs, only at the tip and at the hub. At these locations the discretization of the continuous vortex sheet into a finite set of horseshoe vortices yields to higher numerical approximations and the fully numerical design method predicts non-zero loads. Consistently also for the self-induced velocities, even if for the axial component some higher discrepancies can be highlighted, the agreement between the design procedures is good, with differences concentrated, again, mainly at the tip and at the hub, where the locally different load distributions have more influence.

3.2 Systematic propeller design

Once the consistency (in terms of optimal load distribution and induced velocities with respect to the well-established Lerbs approach) of the fully numerical design code has been confirmed, a total of six different propellers have been designed, considering all the possible permutations of the lifting line and lifting surface corrections methods, with and without hub effects. So at first propeller variants A and AH were designed with the numerical lifting line method with and without the hub image model. Subsequently lifting surface corrections have been applied with the parametric formulation of van Oossanen (1968) (MS) or with the fully numerical lifting surface model (LS), in its turn, with and without the inclusion of the hub effect (suffix H).

Names of the different propellers variants are listed in Table 1. It is clear that some of these variants are obtained with non-consistent theoretical methods (AH-MS, AH-LS, A-LSH) but have been considered and are anyhow presented in the following section, because unfortunately they still have a correspondence with truly design cases among propeller designers. A side scope of the paper is also to offer indication about consequences of an inconsistent application of design codes.

Table 1: Propeller design variants.

Propeller ID	Design Method	L.S. Corrections
A-MS	<i>L.L. w/o hub images</i>	<i>Morgan-Silovic-Denny</i>
AH-MS	<i>L.L. with hub images</i>	<i>Morgan-Silovic-Denny</i>
A-LS	<i>L.L. w/o hub images</i>	<i>Lifting Surface w/o hub</i>
AH-LS	<i>L.L. with hub images</i>	<i>Lifting Surface w/o hub</i>
A-LSH	<i>L.L. w/o hub images</i>	<i>Lifting Surface with hub</i>
AH-LSH	<i>L.L. with hub images</i>	<i>Lifting Surface with hub</i>

All propeller variants have been designed with the moderately loaded assumption for a thrust coefficient of $K_T=0.278$, imposed at an advance coefficient $J=1.2$ and a cavitation index (based on the propeller rate of revolution and shaft depth) $\sigma_N=1.9$. The hub diameter is 20% the propeller diameter. A given balanced skew distribution, typical of modern propellers has been adopted. At the inner radial sections, skew angles are partially outside the range of application of the Van Oossanen lifting surface parametric corrections. A standard NACA 16 thickness distribution, with $a=0.8$ camber line has been chosen.

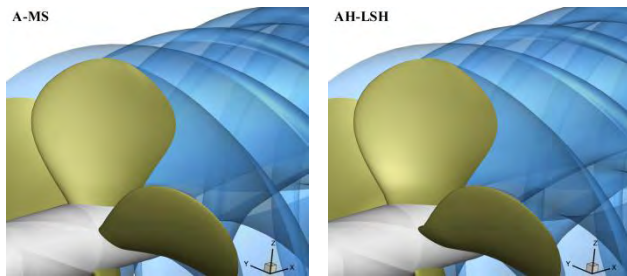


Figure 5: Geometry of two propeller designs.

4 RESULTS

Results from the design activity, in terms of load distributions, are shown in figure 6. As expected, propellers designed without the hub effect show an almost (for numerical reasons discussed in the previous section) zero circulation value at hub radius, whereas the bound vorticity increases rather significantly due to hub effect starting from $r/R=0.4$. From a geometrical point of view only pitch and camber distributions are compared: having designed all the six propellers with the same skew and rake distributions and with the same criteria in terms of cavitation avoidance, the difference in chord and maximum thickness distributions are very similar.

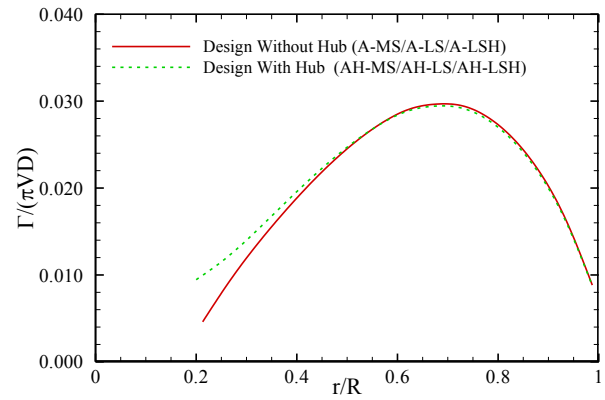


Figure 6: Optimum load distributions for propeller designed with (AH) and without hub effects (A).

Pitch and camber distributions of propellers designed without the hub effect are presented in figures 7 and 8, respectively. Corrections obtained by numerical lifting surface method (with and without hub) appear very similar except at the inner radii where the presence of the hub (case A-LSH) in the model forces a drastic reduction of pitch and camber distributions to ensure a zero-circulation at hub radius. At outer radii, the influence of the hub on the lifting surface corrections results in a slight increase in pitch and camber distributions.

A similar comparison is presented in figure 9 and 10 for the pitch and camber distribution of the following group of propeller designs all sharing the same lifting line design with hub effect (AH-). In this case while consistent numerical lifting surface corrections (with hub effect) result in a local reduction of pitch and camber at the inner radii, as shown in propeller AH-LSH, the numerical lifting surface model without hub effect inconsistently forces an opposite sharp increase of pitch and camber at the same sections, to compensate the higher induced angles of attack there.

Remarkably different corrections to pitch and camber derive from the application of the van Oossanen parametric methods (MS) in both design variants (with and without hub effect: A- and AH-). The main trend is qualitatively similar to the corrections obtained by the numerical lifting surface method, but the absolute values of resulting pitch and camber differ, especially at the tip and root: the maximum camber is slightly over-corrected, while the pitch ratio is slightly under-corrected. The difference is more evident in the case of propeller designs with the hub effect. A role could be played also by the skew distribution that, as already mentioned, is outside the limits of validity of the parametric corrections, especially at the hub. A better measure of the consequences that difference in pitch and camber distributions play on propeller performance and local hydrodynamic characteristics, comes from the analyses of the designs with the potential flow methods and the fully viscous turbulent flow solver.

The correct alignment of blade sections at the inner radii can be inferred by the analysis of the pressure distributions calculated on a blade section close to the

hub, at $r/R = 0.22$, as illustrated in figures 11 to 13 for the designs without hub effects and in figures 14 to 16 for those with hub effects. Predictions obtained by the 3D panel method and the RANSE solver are rather close excepted made for the pressure recovery at the trailing edge, where viscosity effects are missing in the potential flow solver. This is consistent with the validations made in different cases, for example in Brizzolara et al. (2008).

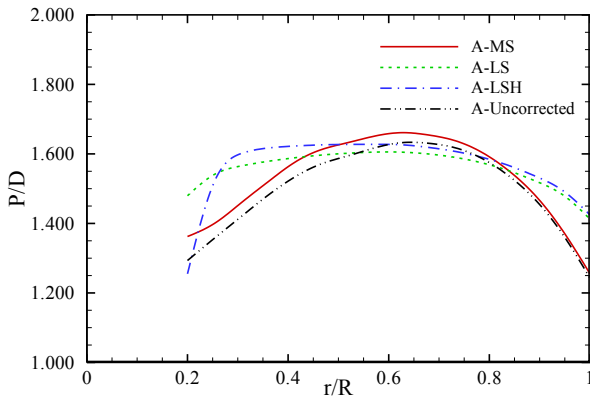


Figure 7: Computed pitch distributions for the propellers designed without hub (A-MS, A-LS and A-LSH).

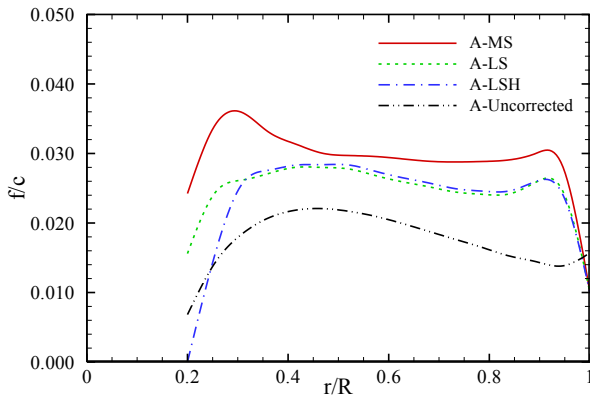


Figure 8: Computed camber distributions for the propellers designed without hub (A-MS, A-LS and A-LSH).

Lower values of pitch combined with a higher camber at inner radii are responsible of pressure diagrams close to inversion: this is the case of propellers designed with the lifting line without hub effect (A-LS or A-LSH). This phenomenon is sharply amplified in the case of the propeller designed with the parametric lifting surface corrections (A-MS). This design, as already noted, presents the highest value of camber with a relatively low value of pitch. A local negative angle of attack at the leading edge of the section at $r/R=0.22$ is predicted by both the panel method and the RANS solver very similarly, while the lifting surface code shows a small, but still positive angle of attack there.

A similar picture is observed for propeller designs with the hub effect (AH- cases). Here the higher lift maintained on the inner sections by the hub allows to maintain higher pitch angles and camber with respect to the previous series of design without hub effect (A- cases). In fact the pressure diagrams show a higher difference between the back and face curves at the leading edge.

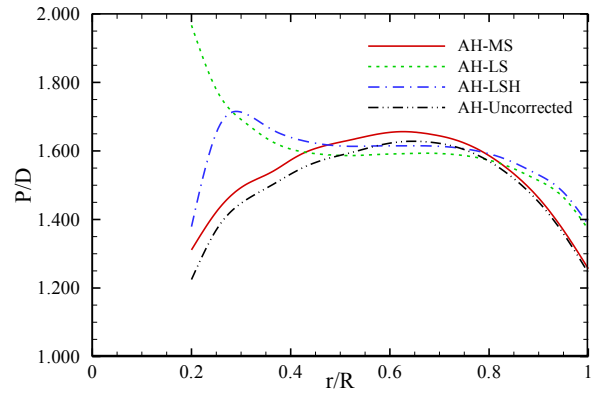


Figure 9: Pitch distributions of propellers designed with hub (AH-MS, AH-LS and AH-LSH).

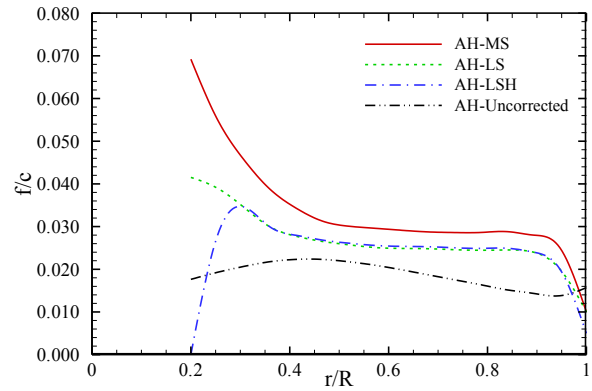


Figure 10: Camber distributions of propeller designs with hub (AH-MS, AH-LS and AH-LSH).

The inconsistent (in this case) camber increase and incorrect pitch reduction obtained by parametric lifting surface corrections (design AH-MS) make the local inversion of angle of attack at the leading edge even more pronounced: the extra loading at hub is almost totally balanced by an excessively high value of camber, while the pitch distribution has a shape similar to the A-MS propeller and values similar to the corrected geometries with the inclusion of the hub.

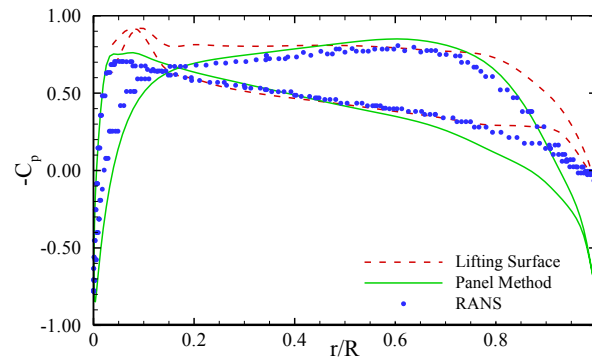


Figure 11: Pressure distribution at hub ($r/R = 0.22$). Propeller A-MS.

The thrust K_T , and torque K_Q coefficients, as well as open water efficiency η_o predicted by the analysis methods are presented in figures 17 to 19, respectively.

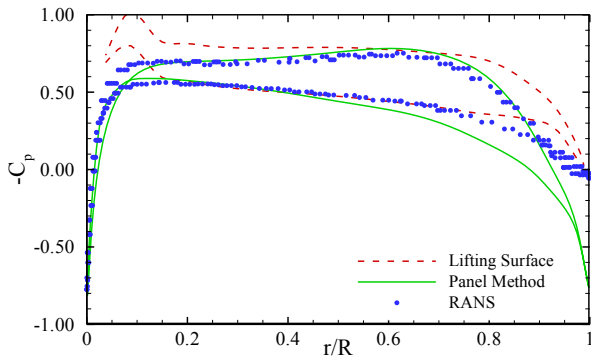


Figure 12: Pressure distribution at hub ($r/R = 0.22$). Propeller A-LS.

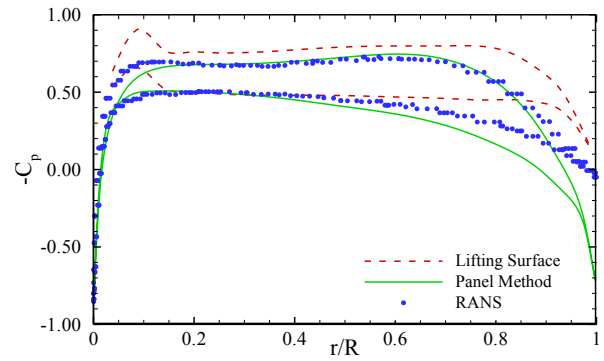


Figure 16: Pressure distribution at hub ($r/R = 0.22$). Propeller AH-LSH.

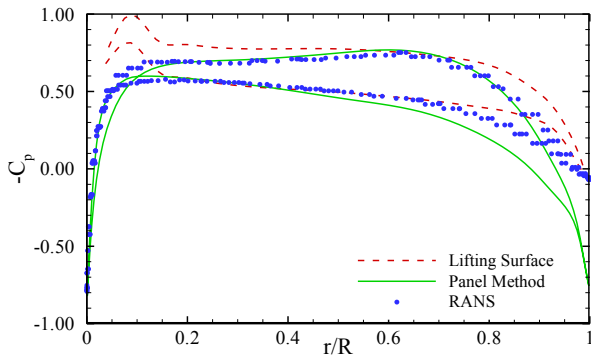


Figure 13: Pressure distribution at hub ($r/R = 0.22$). Propeller A-LSH.

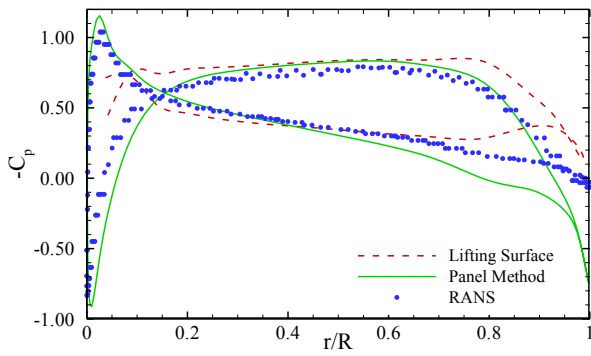


Figure 14: Pressure distribution at hub ($r/R = 0.22$). Propeller AH-MS.

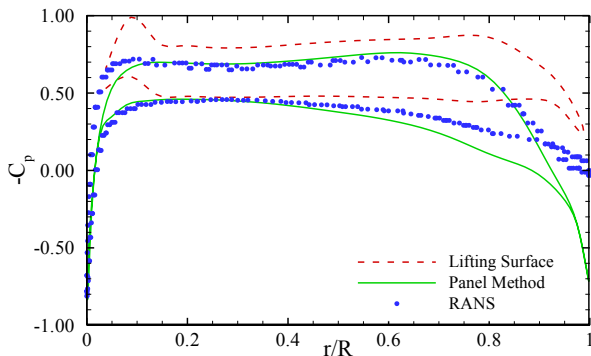


Figure 15: Pressure distribution at hub ($r/R = 0.22$). Propeller AH-LS.

The three potential flow methods do not differ much between themselves in terms of global results in all propeller design cases. Potential flow based predictions of thrust stay within a $\pm 3\%$ error with respect to the design input value. In general the lifting surface analysis methods (LS and LSH) predicts slightly higher thrust values than the panel method and the L.S. with hub effect is generally lower than the one without hub effect and gets very close to the predictions made with the panel method.

The torque predicted with the lifting surface methods is always significantly higher than that predicted by the panel method: this is due to the different friction corrections adopted in the two potential flow methods.

Estimation of thrust and torque performed by the RANSE solver are in general always few points lower than those obtained with the panel method, the difference being more important on the torque values.

The lower values of thrust and torque predicted with RANSE compensate each other in the calculation of open water efficiency that gets very close to that predicted by the panel method, though always one or two points lower. The higher overestimation of the torque values makes efficiencies estimated by the lifting surface method always few points lower than the others.

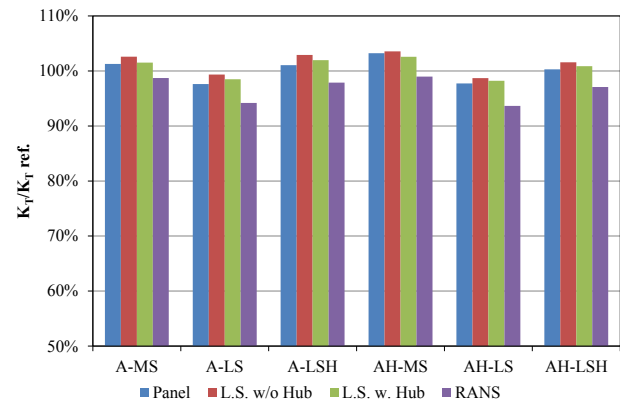


Figure 17: Computed thrust for the designed propellers.

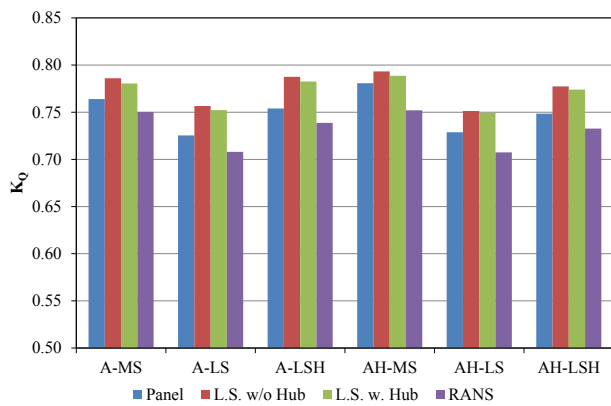


Figure 18: Computed torque for the designed propellers.

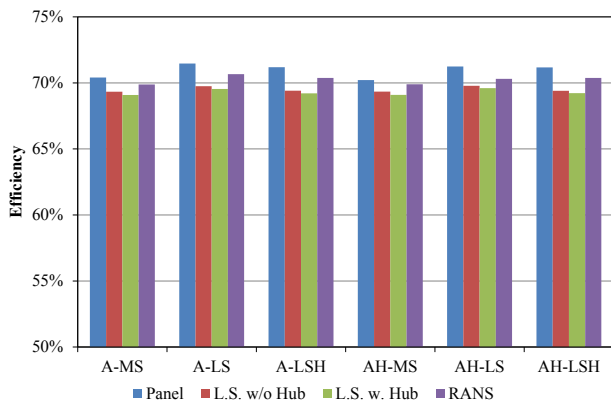


Figure 19: Computed efficiency for the designed propellers.

If the RANSE solver is taken as the reference solver the thrust produced by the designed cases is always sufficiently (for engineering purposes) to the design value, except for cases A-LS and AH-LS, whose predicted thrust is about 6-7% below the required one.

In the framework of potential flow solvers the designed propellers without hub (A-) have a slightly higher delivered thrust than the others with hub effect (AH-). The consistent case A-LS shows about 3% lower than the prescribed value. As expected, predicted values from the lifting surface code including the influence of the hub are closer to the geometrical exact solutions provided by the panel method. The influence of the hub is more evident if the pressure diagrams are taken into account.

In conclusion, the theoretically most consistent design case, AH-LSH, in which the propeller is designed using the numerical lifting surface corrections with the hub effect shows the best overall performance, in terms of local flow near hub sections as well as in terms of matching the design thrust and obtaining the highest efficiency.

6 CONCLUSIONS

A comparison between several design tools and analysis code has been carried out taking into account for hub effect on resulting blade geometries. A coherent and straightforward hub model has been introduced into design procedures and, where possible, into analysis tools.

A practical design case has been discussed proving that consistent design methods lead to proper blade geometries

not only in terms of overall propeller hydrodynamic thrust and torque coefficients but also in terms of local flow, avoiding undesirable phenomena, like inversion of the local angle of attack at the leading edge of hub sections, where traditional parametric corrections largely fail when applied to modern propeller geometries. Propeller designers should have this picture in mind when applying different theoretical methods in propeller design and analysis.

The systematic analysis of local and global hydrodynamic characteristics also confirmed that the best overall performance is achieved by the most consistent design case AH-LSH. Unfortunately most propeller designers are still nowadays not using such consistent methods during the whole design, optimization and analysis process.

The systematic comparison of predictions obtained with different analysis methods evidenced also a need of further refinement of the friction corrections used in the potential flow solvers, especially in the lifting surface code. Future studies of this kind should consider more extreme skew distributions and the cavitation predictions.

7 REFERENCES

- Anderson, P. (1997). 'A comparative study of conventional and tip-fin propeller performances', Proceedings of the 21st Symposium on Naval Hydrodynamics, pp. 930-945, Trondheim, Norway.
- Bertetta D., Brizzolara S., Canepa E., Gaggero S. and Viviani M. (2012). 'EFD and CFD characterization of a CLT propeller', International Journal of Rotating Machinery, Volume 2012, Article ID 348939, p.1-23, ISSN: 1023-621X (Print), ISSN: 1542-3034 (Online), DOI:10.1155/2012/348939.
- Bertetta, D., Brizzolara, S., Gaggero, S., Viviani, M., Savio, L. (2012). 'CP propeller cavitation and noise optimization at different pitches with panel code and validation by cavitation tunnel measurements', Ocean Engineering (2012), ISSN 0029-8018, Elsevier, doi: 10.1016/j.oceaneng.2012.06.026.
- Brizzolara S., Villa D. and Gaggero, S., (2008). 'A systematic Comparison between RANSE and Panel Methods for Propeller Analysis', Hydrodynamics VIII, 8th International Conference on Hydrodynamics, ICHD 2008, Nantes, Oct. 2008, NANTES, vol. 1, p. 289-302.
- Brizzolara, S. and Gaggero, S. (2009). 'Parametric CFD Optimization of Fast Marine Propellers', 10th International Conference on Fast Sea Transportation, FAST2009, Athens, Greece.
- Brizzolara, S., Grassi, D. and Tincani, E. (2012). 'Design method for contra-rotating propellers for high-speed crafts: revising the original Lerbs theory in a modern perspective', International Journal of Rotating Machinery, Vol. 12.
- CD-Adapco (2010). 'StarCCM+, v7.04.06 User's manual', CD-Adapco.

- Coney, W.B. (1989). 'A Method for the Design of a class of Optimum Marine Propellers', Ph.D. thesis, Massachusetts Institute of Technology, USA.
- Eckhardt, M.K. and Morgan, W.B. (1955). 'A Propeller Design Method', Transaction of the Society of Naval Architects and Marine Engineers, Vol. 60, pp. 325-374.
- Gaggero, S. and Brizzolara, S. (2009). 'A panel method for trans-cavitating marine propellers', Proceedings of the 7th International Symposium on Cavitation, Ann Arbor, Michigan, USA.
- Gaggero, S., Grassi, D., and Brizzolara, S. (2011), 'From single to multistage marine propulsor: a fully numerical design approach', Second International Symposium on Marine Propulsors, Hamburg, Germany.
- Grassi, D. and Brizzolara, S. (2007), 'Numerical analysis of propeller performance by lifting surface theory', Proceedings of the 2nd International Conference on Marine Research and Transportation, Ischia, Italy.
- Greeley, D.S. and Kerwin, J.E. (1982). 'Numerical Methods for Propeller Design and Analysis in Steady Flow', Transaction of the Society of Naval Architects and Marine Engineers, 90: 415-453
- Kerwin, J.E. and Leopold, R. (1964). 'A design theory for subcavitating propellers', Transaction of g Society of Naval Architects and Marine Engineers, 72.
- Kerwin, J.E. (2007). 'Hydrofoils and Propellers', MIT Course 2.23 notes.
- Kerwin, J.E., Coney, W.B. and Hsin, C.Y. (1986). 'Optimum Circulation Distributions for Single and Multi-Component Propulsors', Twenty-First American Towing Tank Conference, pp. 53-62.
- Kimball, R.W. and Epps, B.P. (2010). 'OPENPROP code suite', Open-source at <http://openprop.mit.edu>.
- Lerbs, H.W. (1952). 'Moderately Loaded Propellers with a Finite Number of Blades and an Arbitrary Distribution of Circulation', SNAME Transactions, Vol. 60, pp.73-123.
- McCormick, B. W. (1955). 'The effect of finite hub on the optimum propeller', Journal of the Aeronautical Sciences, 22, 9, 645-650.
- Morino, L. and Kuo, C.C. (1974). 'Subsonic Potential Aerodynamic for complex configuration: a general theory', AIAA Journal, 12(2) pp. 191-197.
- Morgan, W.B., Silovic, V. and Denny, S.B. (1968). 'Propeller Lifting-Surface Corrections', Transactions of the Society of Naval Architects and Marine Engineers, Vol. 76, pp. 309-347.
- Sanchez Caja, A. (1988). 'On the Optimum Propeller Loading with Inclusion of Duct and Hub', Master Thesis, Massachusetts Institute of Technology, USA.
- Sanchez-Caja, A., Rautaheimo, P., and Siikonen, T. (2000). 'Simulation of incompressible viscous flow around a ducted propeller using a RANS equation solver', Twenty-Third Symposium on Naval Hydrodynamics, Val de Reuil, France.
- Tachmindji, A. J. (1956). 'The potential problem of the optimum propeller with finite hub', International Shipbuilding Progress, 3, 27, pp. 563-572.
- Tachmindji, A. J., Milam, A. B. (1957). 'The calculation of circulation distribution for propeller with finite hub having three, four, five and six blades', International Shipbuilding Progress, 4, 37, pp. 467-475.
- Tincani, E., Grassi, D. and Brizzolara, S. (2008), 'A design method for contrarotating propellers based on exact lifting surface corrections', 6th International Conference on High Performance Marine Vehicles, vol. 1, pp. 201-214, Naples, Italy
- Wang, M.H. (1985). 'Hub effects in propeller design and analysis', Ph.D. thesis, Massachusetts Institute of Technology, USA.
- VanOossanen, P. (1968). 'Calculation of performance and cavitation characteristics of propellers including effects of non-uniform flow and viscosity', Technical report, Netherland Ship Model Basin.